Available online at www.sciencedirect.com
SCIENCE DIRECT®
Journal of Power Sources 136 (2004) 45–54
JOURNAL OF POWER SOURCES
www.elsevier.com/locate/jpowsour

Modelling study of CO_2 poisoning on PEMFC anodes

G.J.M. Janssen*

Energy research Centre of the Netherlands ECN-Fuel Cell Technology, P.O. Box 1, 1755 ZG Petten, The Netherlands

Received 12 January 2004; received in revised form 26 April 2004; accepted 4 May 2004

Available online 3 July 2004

Abstract

The CO_2 poisoning effect on anodes for the proton-exchange-membrane fuel cell (PEMFC) was examined by model studies. It was assumed that the reverse water gas shift reaction (RWGS) is the origin of the CO_2 poisoning effects. The relation between the anode polarisation losses and the catalytic properties of the catalyst was investigated with a kinetic model and with a fuel cell model including finite utilisation of the fuel. It was found that the main effect of the occurrence of the reverse water gas shift reaction is that a large part of the catalytic surface area becomes inactive for hydrogen dissociation. Desorption of CO formed by reduction of CO_2 followed by transport down the anode gas channel and subsequent re-adsorption on the catalyst was shown to play a minor role. In reformate gas, where besides CO_2 traces of CO are present, CO_2 poisoning will have the largest effect when the CO content is small and at relatively low current density.

Keywords: PEM fuel cell (PEMFC); CO_2 tolerance; Reverse water gas shift reaction; Reformate; Modelling study

1. Introduction

For a low temperature proton-exchange-membrane fuel cell (PEMFC) pure hydrogen is the preferred fuel. However, H_2 has a low energy density and at present there is no infrastructure for hydrogen distribution and storage on a large scale. Conventional fuels like gasoline, natural gas or methanol do not have these disadvantages. In order to be used in a fuel cell they have to undergo a reforming process. In the reforming process the fuel is converted by water or air to a mixture of hydrogen, carbon dioxide, nitrogen and water, and trace amounts of other compounds among which carbon monoxide is most important. The efficiency of the system is affected by this reforming process, not only because of the reforming reaction itself but also because the operation of the PEMFC on reformate gas is less efficient than the operation on pure H_2.

The detrimental effect of small amounts (ppm level) of CO on the cell performance is well known. The presence of inert, non-condensing gases like nitrogen results in additional dilution effects that increase with utilisation [1,2]. Carbon dioxide, which is present in the order of 25%, also contributes to this dilution and utilisation loss, but it has often been recognised [3–5] that the effects are larger than those of an equivalent amount of nitrogen, i.e. that in a fuel cell CO_2 is not inert.

Reduction of CO_2 on Pt by Pt hydrides in acidic solutions in the 0–250 mV versus NHE region was already reported by Giner [6]. The product was found to be a species resembling CO adsorbed on Pt. Further work has shown that the reduction of CO_2 needs the presence of hydrogen atoms adsorbed on the catalyst surface [4,5] but that the reaction can also take place as a normal surface reaction, i.e. not as an electrochemical reaction [3]. It has been assumed that the reaction taking place is the so-called reverse water gas shift reaction (RWGS) in the form:

$$CO_2 + 2M - H \Rightarrow M - CO + H_2O + M$$

where M represents a catalyst site. The adsorbed hydrogen can be formed by electrochemical reduction:

$$H^+ + e + M \Rightarrow M - H$$

or by a chemical (Tafel) reaction:

$$H_2 + 2M \Rightarrow 2M - H$$

In a fuel cell operating at slightly positive anode potentials (order 50 mV) and with hydrogen-rich gas supplied at the anode side the chemical pathway will probably prevail. In the form written above the product species besides water is adsorbed CO. Whereas there is no doubt that the product is a species adsorbing on the catalyst surface, there is

* Tel.: +31 224 564803; fax: +31 224 568489.
E-mail address: janssen@ecn.nl (G.J.M. Janssen).

0378-7753/$ – see front matter © 2004 Elsevier B.V. All rights reserved.
doi:10.1016/j.jpowsour.2004.05.004

Nomenclature

b_c	Tafel slope of the CO electro-oxidation reaction (V)
b_h	Tafel slope of the H electro-oxidation reaction (V)
f	molar flow rate of the fuel times $2F$ ($A\,cm^{-2}$)
F	Faraday constant (96,485 $C\,mol^{-1}$)
I^{av}	average total current density in the cell ($A\,cm^{-2}$)
I^{CO}	local generated current density from CO-electrochemical oxidation ($A\,cm^{-2}$)
I^{H}	local generated current density from H-electrochemical oxidation ($A\,cm^{-2}$)
I^{loc}	local current density at position w in the cell ($A\,cm^{-2}$)
K_1, K_2,K_3, K_4, K_5	parameters for V_{st}
k_a	H_2 adsorption rate constant times $2F$ ($A\,cm^{-2}\,bar^{-1}$)
k_{ac}	CO adsorption rate constant times $2F$ ($A\,cm^{-2}\,bar^{-1}$)
k_d	H_2 desorption rate constant times $2F$ ($A\,cm^{-2}$)
k_{dc}	CO adsorption rate constant times $2F$ ($A\,cm^{-2}$)
k_{ec}	CO pre-exponential electrochemical oxidation rate ($A\,cm^{-2}$)
k_{eh}	H pre-exponential electrochemical oxidation rate ($A\,cm^{-2}$)
k_{rs}	rate constant of the reverse water gas shift reaction ($A\,cm^{-2}$)
n_{CO_2}	molar CO_2 flow rate times $2F$ ($A\,cm^{-2}$)
pX	partial pressure of gas X (bar)
R	gas constant (8.31 $J\,K^{-1}\,mol^{-1}$)
T	cell temperature (K)
u, u'	total fuel utilisation and utilisation at position w
V_{st}	cell voltage excluding anode losses (V)
w	dimensionless position along gas channel (0 = inlet, 1 = outlet)
x_{CO}	molar fraction of CO in the fuel
x_H	molar fraction of H_2 in the fuel
x_{CO_2}	molar fraction of CO_2 in the fuel

Greek letters

η	anode overpotential: potential difference between the electron conducting phase and the proton conducting phase in the anode (V)
θ_H	fraction of the catalytic surface area covered by H
θ_{CO}	fraction of the catalytic surface area covered by CO
ρ	molar area density of catalysts sites ($mol\,cm^{-2}$)

some discussion regarding the true nature of the adsorbate [7–9]. However, it seems it is closely related to adsorbates occurring in the adsorption and electro-oxidation of CO and methanol.

CO_2 is not as strong a poison for the fuel cell as CO. With Pt electrodes and 25% CO_2 in H_2, Wilson obtained cell performance losses much smaller than found with 20 ppm CO in H_2 [3]. Although this shows that CO_2 poisoning is a minor source of performance losses compared to CO, it can still be significant in those cases where due to good fuel processing systems the CO content is small (<10 ppm). Moreover, the sensitivity towards CO_2 is not the same for all catalysts. In our own laboratory we observed that on PtRu the effects were smaller than on Pt [5], whereas on PtMo the effects were substantially larger [10]. Similar trends were observed elsewhere [11,12]. Notice also that effects of CO_2 cannot be eliminated with an air-bleed [1].

The RWGS reaction described above can in principle provide two sources of anode poisoning in a fuel cell. First there is the reduced CO_2, that, in the form of CO or a related species, blocks the catalyst surface for hydrogen dissociation and oxidation. In addition, CO formed by CO_2 reduction can desorb from the surface, enter the gas flow and re-adsorb further down-stream. Thermodynamic calculations have shown that, depending on the water content and temperature, CO concentrations of up to 200 ppm can be achieved in a reformate mixture [5,13]. In practice concentrations would be smaller and depend on the gas flow. If the second mechanism were dominant it would be expected that a more CO tolerant catalyst would also be more CO_2 tolerant. The example of PtMo, already referred to above, shows that this is not the case [10–12]. On PtMo anode losses induced by CO_2 were larger than would be caused by the maximum concentration of CO that could be formed thermodynamically [10].

In order to investigate further the mechanism of CO_2 poisoning, as well as the interplay with the CO tolerance mechanisms displayed by various catalysts, model studies were carried out for the anode of a PEM fuel cell fed on reformate. To this end we have combined the model of Springer [2], which describes the kinetics of H_2 electro-oxidation in the presence of CO, as well as dilution and CO-oxidation effects, with the model for CO_2 reduction suggested by Bellows et al. [4].

2. Theory

2.1. Kinetics

At an anode operating under reformate feed a couple of reactions can take place. The most important one is the dis-

sociative adsorption and electrochemical oxidation of hydrogen. In addition CO adsorbs on the catalyst surface area, where it can be electro-oxidised by water. Finally the CO_2 present can react with adsorbed hydrogen. The model used here was based on the following set of reactions:

Reaction	Forward rate constant	Backward rate constant	
$H_2 + 2M \Leftrightarrow 2M-H$	k_a	k_d	I
$2M-H \Rightarrow 2H^+ + 2e + 2M$	k_{eh}		II
$CO + M \Leftrightarrow CO-M$	k_{ac}	k_{dc}	III
$M-CO + H_2O \Rightarrow CO_2 + 2H^+ + 2e + M$	k_{ec}		IV
$CO_2 + 2M - H \Rightarrow M-CO + H_2O + M$	k_{rs}		V

Reactions (I) and (II) represent the Tafel–Volmer mechanism for hydrogen oxidation. The CO adsorption and desorption was modelled by a simple Langmuir process, based upon the adsorption of one CO per catalyst site. For simplicity the rate constants of the reactions (I) and (III) were not taken to be dependent on the fractional CO coverage of the site, unlike in Springer's model [2]. The CO oxidation by water is represented here by as a single step, although in general it will be at least a two step process involving the formation of adsorbed OH that subsequently oxidises the adsorbed CO. The CO_2 reduction reaction is treated as suggested by Bellows et al. [4], i.e. adsorbed CO represents the CO_2 reduction product. Notice that the electrochemical oxidation of CO (IV) can be considered as the backward reaction of reaction (V).

Like in Springers work the rate constants of the adsorption reactions, k_a, k_{ac}, k_{rs} will be expressed in A/cm^2 (geometric).bar. The other rate constants are in A/cm^2. The reaction constants for the reactions (I), (III), (V) include a factor twice the Faraday constant, as 1 mol of gas is in principle equivalent to two reacting electrons. The rates of electrochemical reactions depend on anode overpotential. For the hydrogen oxidation a hyperbolic sine function was used, allowing zero current density at zero overpotential. The CO oxidation rate was expressed by a normal Tafel behaviour. Throughout this work we assume water saturation of the gas phase, so the water partial pressure is constant and can be incorporated in k_{ec}. When ρ represents the molar area density of catalyst sites and F the Faraday constant the following equations result for the fractional hydrogen and CO coverage:

$$F\rho\frac{d\theta_H}{dt} = k_a pH_2(1-\theta_H-\theta_{CO})^2 - k_d\theta_H^2 - k_{rs}pCO_2\theta_H^2 - 2k_{eh}\theta_H \sinh\frac{\eta}{b_h} \quad (1)$$

$$2F\rho\frac{d\theta_{CO}}{dt} = k_{ac}pCO(1-\theta_H-\theta_{CO}) - k_{dc}\theta_{CO} + k_{rs}pCO_2\theta_H^2 - 2k_{ec}\theta_{CO}\exp\frac{\eta}{b_c} \quad (2)$$

The current densities are:

$$I_H = 2k_{eh}\theta_H \sinh\frac{\eta}{b_h}, \quad I_{CO} = 2k_{ec}\theta_{CO}\exp\frac{\eta}{b_c}, \text{ and } I = I_H + I_{CO} \quad (3)$$

In the stationary state the left-hand side of the Eqs. (1) and (2) becomes zero and they can be written as:

$$0 = k_a pH_2(1-\theta_H-\theta_{CO})^2 - k_d\theta_H^2 - k_{rs}pCO_2\theta_H^2 - 2k_{eh}\theta_H\sinh\frac{\eta}{b_h} \quad (4)$$

$$\theta_{CO} = \frac{k_{ac}pCO(1-\theta_H)}{k_{ac}pCO + k_{dc} + k_{ec}\exp(\eta/b_c)} + \frac{k_{rs}pCO_2}{k_{ac}pCO + k_{dc} + k_{ec}\exp(\eta/b_c)}\theta_H^2 \quad (5)$$

By substituting Eq. (5) into Eq. (4) θ_H can be solved as one of the real roots of a fourth-order polynomial, with the conditions:

$$0 \le \theta_H \le 1, \quad 0 \le \theta_{CO} \le 1, \text{ and } \theta_H + \theta_{CO} \le 1 \quad (6)$$

For further reference we consider here two special cases:

(1) No CO_2 in the fuel. This is the same case as treated by Springer. Eq. (5) reduces to:

$$\theta_{CO} = \frac{k_{ac}pCO(1-\theta_H)}{k_{ac}pCO + k_{dc} + k_{ec}\exp(\eta/b_c)} \quad (7)$$

Notice, that if there is no desorption or oxidation of CO the final result of solving (4) and (7) would be $\theta_H = 0$, $\theta_{CO} = 1$. If there is only desorption of CO (and no electrochemical oxidation) there is a limiting value for θ_{CO}, attained when $\theta_H = 0$:

$$\theta_{CO}^{max} = \frac{pCO}{pCO + k_{dc}/k_{ac}} \quad (8)$$

and a corresponding limiting current density:

$$I_H^{lim} = k_a pH_2\left(\frac{k_{dc}/k_{ac}}{k_{dc}/k_{ac} + pCO}\right)^2 \quad (9)$$

(2) No CO in the fuel. In this case, Eq. (5) reduces to:

$$\theta_{CO} = \frac{k_{rs}pCO_2}{k_{dc} + k_{ec}\exp(\eta/b_c)}\theta_H^2 \quad (10)$$

Also in this case without desorption and oxidation of CO the stationary state solutions would be $\theta_H = 0$, $\theta_{CO} = 1$. Again, if there is desorption of CO, and no electro-oxidation a limiting current density would arise at $\theta_H = 0$. However, since in that case also $\theta_{CO} = 0$ (Eq. (10)) this limiting current density is equal to one obtained without CO or CO_2:

$$I_H^{lim} = k_a pH_2 \quad (11)$$

2.2. Utilisation of the fuel

There are several ways in which CO_2 will affect the performance if it is present in the anode feed of a fuel cell. Apart from surface blocking, as indicated above in the kinetic model, the dilution and utilisation of hydrogen lead to a reduced partial hydrogen pressure and hence increased activation and Nernst losses. In this respect, the addition of CO_2 is equivalent to the addition of N_2. Moreover, CO formed in the CO_2 reduction process can desorb into the gas flow. The concentrations that can be attained will increase with decreasing gas flow, i.e. with increasing utilisation of the flow. This CO can cause poisoning further down the channel. In the present work, the kinetic model described above is combined with an integration of the current density over the flow channel, as described in [2], but with a slight modification to accommodate the effects of the water gas shift reaction. When the partial pressures in the gas channel are a function of the position in the channel, the current density becomes a function of the position in the channel. Since the cell potential is constant along the channel, this means the anode overpotential is also a function of the position in the channel. The anode overpotential is calculated by:

$$\eta^{\mathrm{loc}} = V_{\mathrm{cell}} - V_{\mathrm{st}}(I^{\mathrm{loc}}) + \frac{RT}{2F}\ln p\mathrm{H}_2^{\mathrm{loc}} \tag{12}$$

The last term in this equation represents the change in Nernst potential along the channel. In this equation V_{st} represents the ohmic losses and the losses at the cathode. For V_{st} the following empirical expression is used, suggested by Kim et al. [14]:

$$V_{\mathrm{st}}(I^{\mathrm{loc}}) = K_1 - K_2\ln(I^{\mathrm{loc}}) - K_3 I^{\mathrm{loc}} - K_4\exp(-K_5 I^{\mathrm{loc}}) \tag{13}$$

In this equation K_1 represents the reversible open cell potential and the cathode activation losses at $I^{\mathrm{loc}} = 1\,\mathrm{A/cm^2}$, K_2 corresponds to the Tafel slope of the oxygen reduction reaction at the cathode and K_3 is a measure for the ohmic resistance of the cell. The last term in Eq. (13) with parameters K_4 and K_5 represents mass transfer losses at the cathode occurring at high current densities.

For a given set of gas conditions it is possible to obtain, in an iterative procedure, a set of consistent values of η, I_{H}, I_{CO}, and $n_{\mathrm{CO_2}}$. The latter variable represents the amount of CO_2 reacting in reaction (V) and is calculated from:

$$n_{\mathrm{CO_2}} = k_{\mathrm{rs}} p\mathrm{CO_2}\theta_{\mathrm{H}}^2 \tag{14}$$

Notice, that $n_{\mathrm{CO_2}}$ is expressed in $\mathrm{A/cm^2}$ (geometric) like I_{H} and I_{CO}, i.e. a factor of twice the Faraday constant ($2F$) is included. The integration of the model over the channel proceeds as follows. The total flow is reduced along the channel as a result of the hydrogen consumption. The nitrogen flow remains unchanged, as does the sum of the CO and CO_2 flows, since one molecule CO reacts to one molecule of CO_2 and vice versa. The total water partial pressure is kept constant, at saturation level. The dry molar flow rate (i.e. excluding water) at any point in the channel is given by:

$$f = f^{\mathrm{in}}\frac{1 - x_{\mathrm{H}}^{\mathrm{in}}}{1 - x_{\mathrm{H}}} \tag{15}$$

For the derivatives of the total molar flow rate and specific molar flow rates we obtain with respect to the dimensionless position in the channel (0 =inlet, 1 =outlet):

$$\frac{\mathrm{d}f}{\mathrm{d}w} = -I_{\mathrm{H}} \tag{16}$$

$$\frac{\mathrm{d}x_{\mathrm{H}}f}{\mathrm{d}w} = -I_{\mathrm{H}} \quad \frac{\mathrm{d}x_{\mathrm{CO}}f}{\mathrm{d}w} = -I_{\mathrm{CO}} + n_{\mathrm{CO_2}} \tag{17}$$

$$\frac{\mathrm{d}x_{\mathrm{CO_2}}f}{\mathrm{d}w} = +I_{\mathrm{CO}} - n_{\mathrm{CO_2}} \quad \frac{\mathrm{d}x_{\mathrm{N_2}}f}{\mathrm{d}w} = 0 \tag{18}$$

In the above equations the molar flow rate incorporates a factor $2F$. For simplicity it is assumed that the change of the total CO_2 flow is small compared to the total flow and may be neglected. To calculate the fraction of CO_2 in the flow the sum of the CO_2 and N_2 flows is calculated and the fraction of CO_2 and N_2 is calculated by keeping the ratio of the respective fractions equal to the inlet ratio. There are now only three variables to be integrated:

$$\frac{\mathrm{d}f}{\mathrm{d}w} = -I_{\mathrm{H}} \quad \frac{\mathrm{d}x_{\mathrm{H}}}{\mathrm{d}w} = \frac{-I_{\mathrm{H}}(1 - x_{\mathrm{H}})}{f}$$
$$\frac{\mathrm{d}x_{\mathrm{CO}}}{\mathrm{d}w} = \frac{-I_{\mathrm{CO}} + n_{\mathrm{CO_2}} + x_{\mathrm{CO}}I_{\mathrm{H}}}{f} \tag{19}$$

In a fuel cell the fuel is usually supplied at a constant utilisation or stoichiometry, i.e. the inlet flow rate f^{in} depends on the average current density and is therefore not known until the average current density is known. As shown in [2] it is possible to perform the integration over the local utilisation u' instead of over the channel length. The relation between the two variables is:

$$(x_{\mathrm{H}}^{\mathrm{in}} + x_{\mathrm{CO}}^{\mathrm{in}})f^{\mathrm{in}}u'(w) = \int_0^w (I_{\mathrm{H}} + I_{\mathrm{CO}})\,\mathrm{d}w \quad \text{or}$$
$$\frac{\mathrm{d}w}{\mathrm{d}u'} = \frac{(x_{\mathrm{H}}^{\mathrm{in}} + x_{\mathrm{CO}}^{\mathrm{in}})f^{\mathrm{in}}}{I_{\mathrm{CO}} + I_{\mathrm{H}}} \tag{20}$$

Using Eq. (20) we now obtain equations for the derivatives of the x_{H} and x_{CO} that can be integrated:

$$\frac{\mathrm{d}x_{\mathrm{H}}}{\mathrm{d}u'} = -\frac{x_{\mathrm{H}}^{\mathrm{in}} + x_{\mathrm{CO}}^{\mathrm{in}}}{1 - x_{\mathrm{H}}^{\mathrm{in}}}\frac{(1 - x_{\mathrm{H}})^2 I_{\mathrm{H}}}{I_{\mathrm{H}} + I_{\mathrm{CO}}} \tag{21}$$

$$\frac{\mathrm{d}x_{\mathrm{CO}}}{\mathrm{d}u'} = -\frac{x_{\mathrm{H}}^{\mathrm{in}} + x_{\mathrm{CO}}^{\mathrm{in}}}{1 - x_{\mathrm{H}}^{\mathrm{in}}}\frac{(1 - x_{\mathrm{H}})(I_{\mathrm{CO}} - n_{\mathrm{CO_2}} - x_{\mathrm{CO}}I_{\mathrm{H}})}{I_{\mathrm{H}} + I_{\mathrm{CO}}} \tag{22}$$

The third variable to be integrated is:

$$\frac{\mathrm{d}w}{\mathrm{d}u'}\left(\frac{1}{(x_{\mathrm{H}}^{\mathrm{in}} + x_{\mathrm{CO}}^{\mathrm{in}})f^{\mathrm{in}}}\right) = \frac{1}{I_{\mathrm{CO}} + I_{\mathrm{H}}} \tag{23}$$

Using a fourth-order Runge–Kutta scheme x_H and x_{co} are calculated as function of the utilisation. After the integration f^{in} can be obtained from:

$$I^{av} = f^{in}(x_H^{in} + x_{CO}^{in})u \quad (24)$$

Using this value of f^{in}, the variable w can now be calculated as a function of u' from the integration of Eq. (23).

3. Results

3.1. No CO in the fuel, zero utilisation

In order to investigate the effect of the reverse water gas shift reaction on the anode polarisation curve, we first consider the case pCO = 0. In a fuel cell this would imply that the anode gas does not contain traces of CO, but also that the utilisation of the fuel is zero. At zero utilisation the flow is infinitely high and therefore the composition is constant, i.e. CO formed in the reverse shift reaction and desorbing according to reaction (III) does not affect the gas composition, nor does the consumption of H_2 and CO_2. The relation between θ_{CO} and θ_H is now given by Eq. (10). Notice, that if there is no oxidation or desorption of CO (k_{ec} and $k_{dc} = 0$) the stationary state will be that all catalytic sites are covered by CO ($\theta_{CO} = 1$, $\theta_H = 0$).

In the first set of calculations we consider the case where electrochemical oxidation of CO does not occur, corresponding to the case of a Pt electrode at low (<0.2 V) overpotential. Desorption of CO, however, was included. The values for the parameters describing the hydrogen oxidation process (reactions I–II) have been chosen such that at normal fuel cell operating conditions the anode losses under pure hydrogen are minimal, i.e. the limiting current density is very high, and result in a realistic hydrogen coverage at low anode overpotential. These values are determined by the ratio k_d/k_a. The parameter k_{eh} was high enough, so that the electrochemical step did not contribute to the losses. The value for the rate constant of the CO adsorption step was chosen arbitrarily, but the ratio of the rate constants of the adsorption and desorption of CO was chosen such that a high CO coverage results already at low CO content. These parameter values have all been listed in Table 1. In this set of calculations the rate constant of the reverse water gas shift reaction, k_{rs}, was varied. Two-non-zero values were chosen, one that resulted in medium coverage of the catalyst surface area and one that resulted in high coverage of the catalytic surface area (see below).

Table 1
Values for the parameters used in the kinetic model

k_a (A/cm^2 bar)	40
k_d	0.5 bar × k_a
k_{eh} (A/cm^2)	4
b_h (V)	0.032
k_{ac} (A/cm^2 bar)	20
k_{dc}	3×10^{-6} bar × k_{ac}
k_{ec} (A/cm^2)	0, 3×10^{-6} or 3×10^{-5} (varied)
b_c (V)	0.06
k_{rs} (A/cm^2 bar)	0, 0.002 or 0.02 (varied)

Eq. (4) with Eq. (10) was solved for a range of values of the anode overpotential η, for a mixture of H_2 and CO_2. This resulted in the polarisation curves plotted in Fig. 1a. For each of the current density values obtained θ_H and θ_{CO} are now also known, they are shown in Fig. 1b and c. These figures show that if the anode is operated under hydrogen with inert CO_2 ($k_{rs} = 0$) the hydrogen coverage only decreases slightly with the current density, at least as long as the current density is far from the limiting current density. When the reverse shift reaction can occur ($k_{rs} \neq 0$) the CO coverage becomes non-zero at stationary conditions, and θ_H drops. The CO

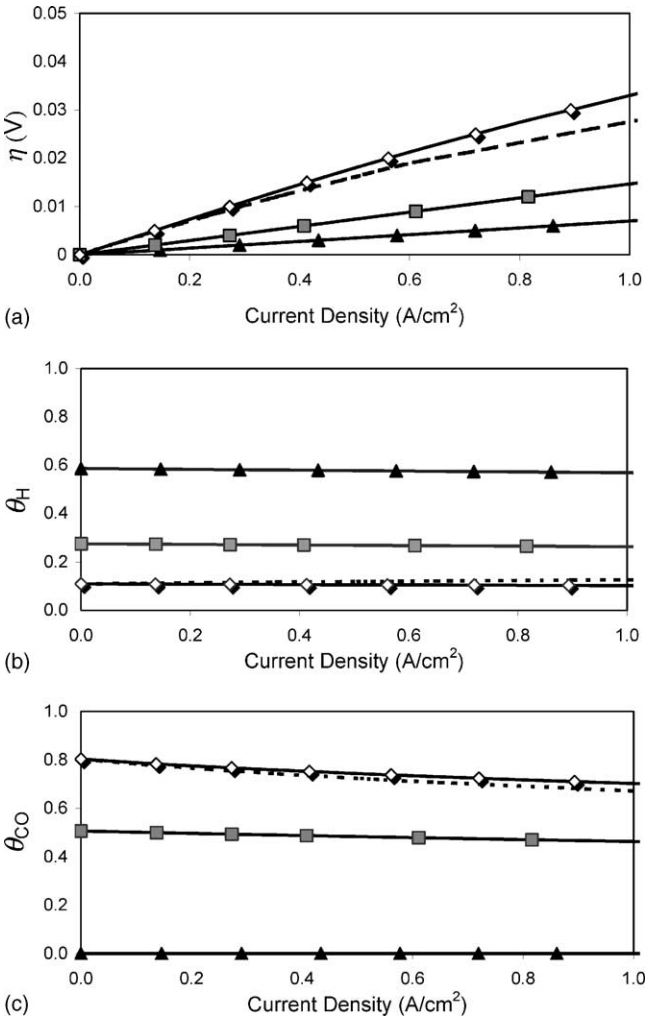

Fig. 1. Results obtained with the kinetic model, $pH_2 = 0.8$ bar, $pCO_2 = 0.2$ bar, pCO = 0, for various values of the rate constant of the RWGS reaction, $k_{rs} = 0$ (▲), 0.002 (■) or 0.02 (◇) A/cm^2 bar. The dashed curves were calculated using $k_{rs} = 0.02$ A/cm^2 bar and $k_{ec} = 3 \times 10^{-5}$ A/cm^2. All other curves were obtained with $k_{ec} = 0$. Other parameter values can be found in Table 1. (a) Shows the overpotential as function of total current density, (b) the fractional coverage of catalytic sites by hydrogen, and (c) the fractional coverage by CO.

coverage θ_{CO} increases with increasing rate of reaction V, i.e. with increasing k_{rs} as illustrated in the Fig. 1c or increasing pCO_2 (see Eq. (10)), or with decreasing k_{dc} (see Eq. (10)). The lower values of θ_H imply that a higher overpotential is needed for the same current density, i.e. increased anode losses. At higher current densities the values of θ_{CO} show a small decrease, consistent with the decrease of θ_H.

The first result of the water gas shift reaction therefore is that part of the catalytic surface area becomes ineffective for the hydrogen oxidation, and the overpotential losses increase. The amount of surface area blocked by CO increases with increasing pCO_2. The fraction blocked further increases with increasing k_{rs}, or with decreasing k_{dc}. Notice that this finite CO-coverage does not require a non-zero value of pCO.

Eq. (10) shows that according to the model the effect of CO electrochemical oxidation is similar to CO desorption. The only difference is that the oxidation rate increases with the overpotential and therefore it mitigates the effects of the RWGS reaction at larger current densities, as is demonstrated by the results in Fig. 1.

3.2. CO in the fuel, zero utilisation

When there is no CO_2 in the fuel, or when the rate constant k_{rs} is zero, this case corresponds to the classical CO poisoning case. When electrochemical oxidation of CO is excluded ($k_{ec} = 0$) then according to Eqs. (8) and (9) a maximum coverage of CO and a corresponding limiting current density occur. In the case of 10, 20 and 50 ppm in a dry gas with pressure 1 bar, the values for the maximum CO coverage calculated with the parameter values from Table 1 are 0.77, 0.87 and 0.94, respectively. With $pH_2 = 0.8$ bar the corresponding limiting current densities are 1.7, 0.54 and 0.10 A/cm^2. The curves presented in Fig. 2 reflect these results. It is also shown that well below the limiting current density the CO coverage is smaller than the maximum value but it increases with the current density when θ_H shows a decline towards zero.

When RWGS reaction is included, the coverage by CO is already at low current densities close to the maximum value. This implies a further reduction of θ_H and an increased value of the overpotential at a given current density. Notice that due to the reduction of θ_H the rate of the CO_2 reduction will also be lower than in the case without CO. Close to the limiting current density the CO coverage attains the same values as in the case of direct CO adsorption. At this current density $\theta_H \to 0$ and the additional effect of CO_2 disappears.

In practice, however, CO will be oxidised when the overpotential becomes sufficiently large. This reduces the overpotential both in the case with and without RWGS reaction, as becomes clear from comparison of Figs. 2 and 3. Fig. 3 also shows that at low current densities the effect of the RWGS reaction is larger than at high current densities. At low current densities the RWGS reaction results again in a CO coverage close to the maximum value given by Eq. (9).

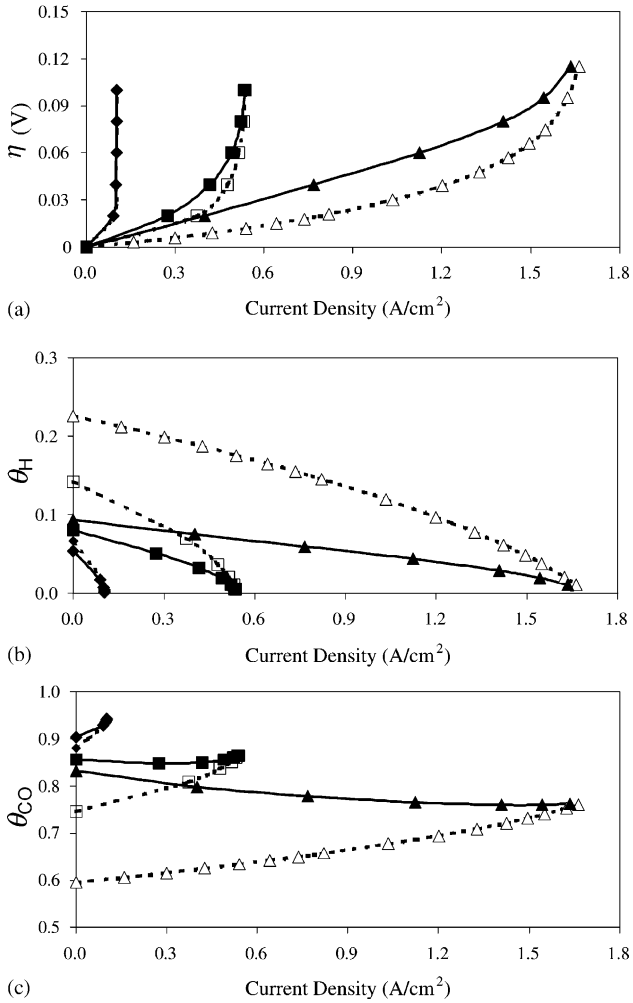

Fig. 2. Curves showing the effect of the reverse shift reaction calculated according to the kinetic model. The gas composition was $pH_2 = 0.8$ bar, $pCO_2 = 0.2$ bar, and pCO 10 μ bar (▲), 20 μ bar (■) or 50 μ bar (◆). The dashed curves with open symbols were obtained with $k_{rs} = 0$, the drawn curves with closed symbols with $k_{rs} = 0.02$ A/cm^2. All curves were calculated with $k_{ec} = 0$. Other parameter values can be found in Table 1. (a) Shows the overpotential as function of total current density, (b) the fractional coverage of catalytic sites by hydrogen and (c) the fractional coverage by CO. Notice that in the case of the highest CO content the curves for the two different k_{rs} values almost coincide.

Without the RWGS reaction the coverage is smaller, similar to what was found in the case without CO oxidation. As the current density and the overpotential increase, the coverage by CO in both cases tends to the same value, e.g. the additional CO_2 poisoning effect disappears.

3.3. Effect of CO_2 in H_2, finite utilisation

The CO_2 sensitivity of an anode can be tested by measuring the performance of a cell operated in H_2 with increasing amounts of CO_2. Here, we present model results obtained for a gas mixture saturated with water at 80 °C, 1.5 bar. A H_2 utilisation of 67% was assumed. To enable comparison with recent experimental data in our laboratory, cell

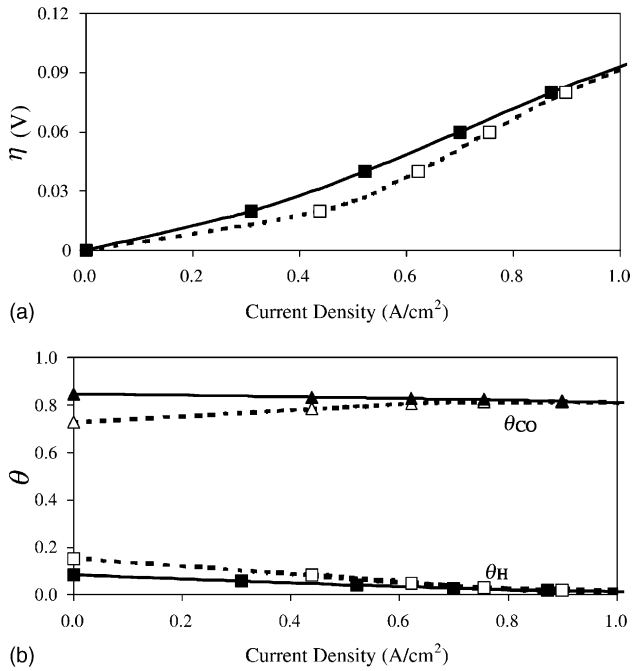

Fig. 3. Results from the kinetic model obtained with $pH_2 = 0.8$ bar, $pCO_2 = 0.2$ bar, and $pCO = 20\,\mu$bar. Electrochemical oxidation of CO was included with $k_{ec} = 3 \times 10^{-6}$ A/cm^2. The dotted lines with open symbols correspond to the case $k_{rs} = 0$, the drawn curves to $k_{rs} = 0.02$ A/cm^2.

performances at a fixed current density were calculated. The anode was modelled with the parameter values from Table 1, the cathode and ohmic losses were calculated using the parameter values from Table 2. The values were obtained by fitting Eq. (13) to an experimental *V–I* characteristic of a cell operated under the above conditions with H_2/air.

In Fig. 4 the effect of increasing CO_2 content is presented. As expected the performance decreases with increasing CO_2 fraction. However, as Fig. 4b shows, the amount of CO in the anode outlet gas decreases with increasing CO_2 content. The main reason for this effect is that the total flow increases when the CO_2 fraction increases, as a result of the fixed hydrogen utilisation. When there is no oxidation of CO the total amount formed in the RWGS reaction can easily be calculated from the outlet concentration. Fig. 4c shows that this amount increases with the CO_2 fraction, as expected. The results can be compared to those obtained with a mixture of $H_2/N_2/CO_2$ where the H_2 flow is constant but N_2 was gradually replaced by CO_2. In that case the flow is constant, but larger than the H_2/CO_2 flow due to the extra nitrogen. The CO concentration at the anode outlet increases slightly

Table 2
Values for the parameters in V_{st} (ohmic and cathode losses).

K_1 (V)	0.756
K_2 (V)	0.024
K_3 (ohm cm^2)	0.173
K_4 (V)	9.29×10^{-4}
K_5 (cm^2/A)	3.1888

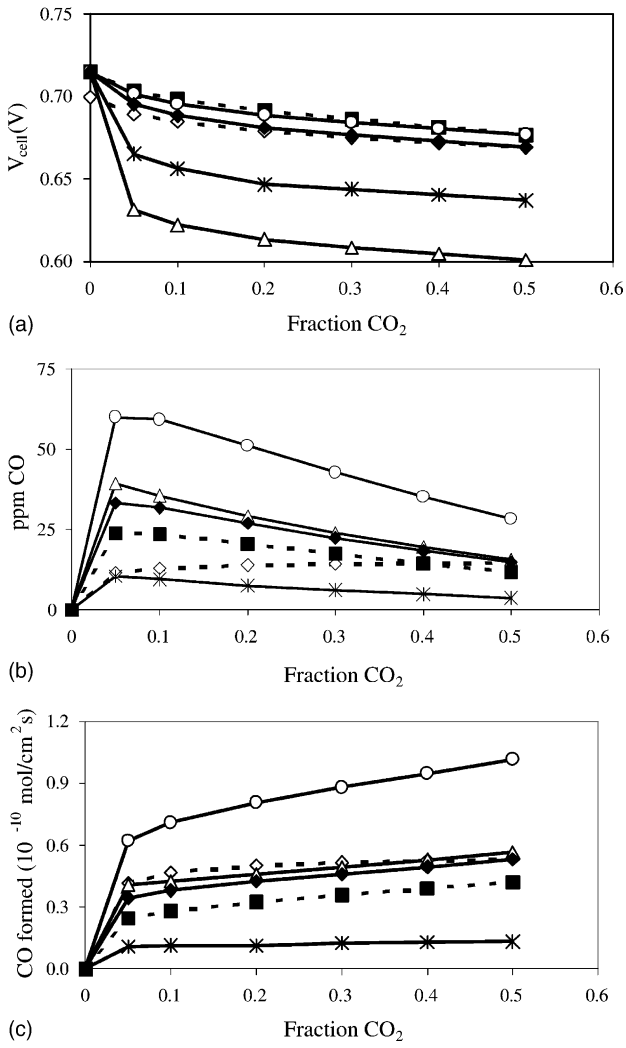

Fig. 4. Cell performance, CO concentration in the anode outlet and rate of CO formation as a function of the CO_2 content in H_2 (or H_2/N_2). The values were obtained at a current density of 350 mA/cm^2, other conditions see text. The base case (◆) was calculated using the parameter values of Table 1 with $k_{ec} = 0$ A/cm^2 and $k_{rs} = 0.02$ A/cm^2 bar and using H_2/CO_2 as feed. The dashed curves with open symbols (◇) were calculated with 50% H_2, the indicated fraction of CO_2, balance N_2. The other curves were calculated as the base case but with, respectively, $100 \times k_{rs}$ (Δ), $0.1 \times k_a$ (∗), $2 \times k_{dc}/k_{ac}$ (○) and $k_{ec} = 3 \times 10^{-6}$ A/cm^2 (■).

as result of the larger pCO_2 but is smaller than in the case of H_2/CO_2 when the flow is smaller. The actual amount of CO formed is larger than in H_2/CO_2, in spite of the smaller fraction of hydrogen. This means that the larger CO concentration in H_2/CO_2 inhibits further reaction of CO_2.

With respect to Fig. 4b it must be noted that the concentrations shown here can be larger than what is expected for thermodynamic equilibrium. In fact the fuel cell conditions are not equilibrium conditions, and the rate constants of the reactions have been chosen such that they reflect certain assumptions concerning the kinetics. The values chosen here imply that the normal water gas shift reaction cannot take place, the activation of water needs a certain overpotential.

When the rate constant of the RWGS reaction is increased by a factor of 100, the performance drops (Fig. 4a). However, Fig. 4b shows that the amount of CO at the outlet is not much affected. This means that similar amounts of CO are being formed as is confirmed by Fig. 4c. As was already shown above, a higher rate constant results in a larger value for θ_{CO} in the stationary state, and this results in a lower value for θ_H. This again reduces the amount of CO formed. Since the actual rate of the RWGS reaction (given by Eq. (14)) depends through θ_H in a complex way on the rate constant k_{rs}, the amount of CO in the outlet is *not* a direct measure for the rate constant of the of the RWGS reaction.

Another parameter that will have a large effect on the CO coverage is the ratio k_{dc}/k_{ac}. Increase by a factor of two results in a decrease of the maximum value for θ_{CO} at, e.g. 10 ppm from 0.77 to 0.62. The effect is an increase of the cell performance (Fig. 4), as lower θ_{CO} results in higher values for θ_H. This also increases the rate of CO formation in the RWGS. The CO content at the outlet is therefore larger than in the case of small k_{dc}/k_{ac} but the net effect is an increase of performance.

Also the dissociation rate of hydrogen will influence the CO_2 poisoning effect. A smaller value for k_a results in an increased performance loss. The main effect of a lower k_a is that θ_H is reduced. This results in a lower rate of formation of CO and lower CO content at the outlet, but not in a reduction of θ_{CO}. Notice, that the effect of this lower k_a on the cell performance is negligible when there is no CO_2 present. It is smaller than the effect of replacing 50% of the H_2 by N_2 as Fig. 4a shows.

The effect of CO poisoning can be mitigated if electro-oxidation of CO is possible, as shown in Fig. 4a. The amount of CO at the outlet also decreases as does the amount of CO formed minus oxidised with respect to the base case.

3.4. Reformate feed, finite utilisation

In order to analyse losses with a typical reformate feed stream containing 40% H_2, 40% N_2, 20% CO_2 and 10 ppm CO, water saturated at 80 °C, and with a pressure of 1.5 bar, several *V–I* curves were calculated with different anode feeds. The ohmic and cathode losses were calculated according to Eq. (13), using the parameter values listed in Table 2. The anode losses were calculated with the kinetic model and parameter values from Table 1 ($k_{ec} = 3 \times 10^{-6}$ A/cm^2, $k_{rs} = 0.02$ A/cm^2). An overall utilisation of 90% was assumed. Fig. 5 shows the results. The difference between the curves obtained with pure H_2 and with H_2/N_2 represents the losses due to dilution and utilisation.

When part of the nitrogen is replaced by CO_2, the cell performance decreases due to catalyst surface blocking as a result of the RWGS reaction and CO formation. With the parameter values chosen here CO_2 poisoning presents an additional loss comparable to the dilution and utilisation loss. Moreover, at current densities below 0.5 A/cm^2 the CO_2 poisoning is comparable to the losses obtained in a feed without CO_2 but with 10 ppm CO. At. At higher current density the rate of CO_2 reduction is reduced due to lower amount of H-adsorbed sites available for the CO_2 reduction reaction, hence at higher current density the effects of 10 ppm CO become larger than those of CO_2.

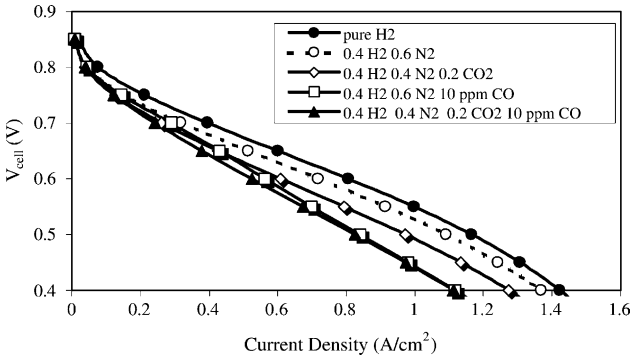

Fig. 5. *V–I* curves calculated with different fuel compositions. Utilisation in all cases 90%. For details of the calculation see text. The numbers of in legend refer to the fraction of the gas species in the total (dry) flow.

In Fig. 6, the CO content in both cases is shown calculated at a cell voltage of 0.6 V. In the case, of no CO in the feed there is a gradual increase of the CO content in the anode channel, until it decreases near the channel exit where the overpotential will be highest and CO electro-oxidation will be faster than CO_2 reduction. In the case of no CO_2 in the feed the CO content drops gradually from the initial value as a result from electro-oxidation. Notice that without electro-oxidation the CO content would increase also in this case.

When both CO_2 and CO are present in the feed, the CO content is on the whole larger than in the cases without CO or without CO_2 and goes through a maximum. In the *V–I* curves at intermediate current density the effect of both CO and CO_2 in the feed is an additional performance loss, but the effect is not additive. Moreover, at high current densities the CO effect seems to prevail, whereas at low current densities the CO_2 effect dominates. This is similar to results obtained with

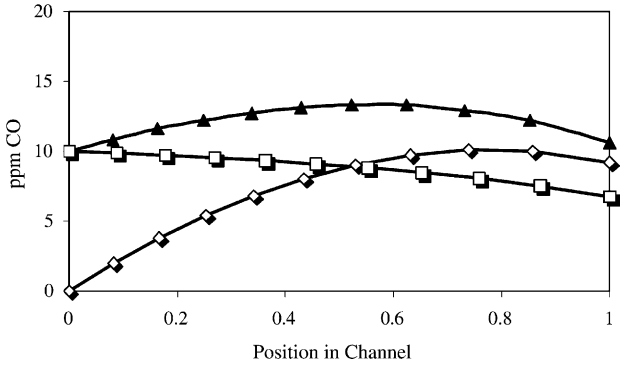

Fig. 6. The CO content as a function of the position in the gas channel in the case of 20% CO_2 in the dry feed but no CO (◇), no CO_2 but 10 ppm CO (□), 10 ppm CO and 20% CO_2 in the feed (▲). The data correspond to point $V_{cell} = 0.6$ V in the previous figure.

the kinetic model and displayed in Fig. 3. In the presence of CO the H-coverage of the catalyst surface area is small and the RWGS reaction is suppressed.

4. Discussion

The above analyses based on a simple model have shown how CO_2 poisoning effects depend on the properties of the anode catalyst material. The most important conclusions are that increase of the rate constant of the RWGS reaction and reduction of the hydrogen dissociation rate enhance CO_2 poisoning effects, whereas CO desorption and CO electro-oxidation mitigate the effect. The amount of CO at the anode outlet does not correlate with the degree of CO_2 poisoning. The main cause of CO_2 poisoning is that there is a stationary high coverage of the catalyst surface area by reduced CO_2, e.g. CO. This reduces the amount of surface area covered by hydrogen, which reduces both the hydrogen oxidation rate as well as the CO formation rate in the RWGS reaction.

Work in our own laboratory, as well as work by others [11,12] has shown that different catalyst materials do indeed respond differently to CO_2. Some results recently obtained in our laboratory are shown in Fig. 7. Notice that the shape of the measured curves resembles well those of the ones calculated using the model. Moreover, the observed anode losses are in the range 0–100 mV, comparing well to those obtained with the range of values used for the model calculations (see Fig. 4). However, given the simplicity of the model and the number of parameters affecting the effect of CO_2 poisoning no attempt will be made here to fit the parameter values of the model to the experimental curves, and only a qualitative interpretation of the observed curves will be given.

Fig. 7 shows that PtRu alloy is more CO_2 tolerant than Pt. It is well established that PtRu alloy is also more CO tolerant than Pt. At low overpotential (<0.2 eV) this is not ascribed to enhanced CO oxidation but to reduced adsorption due to the ligand effect [15,16]. According to the model analyses presented here this would explain a higher CO_2 tolerance. In this case the expected CO content in the anode outlet would

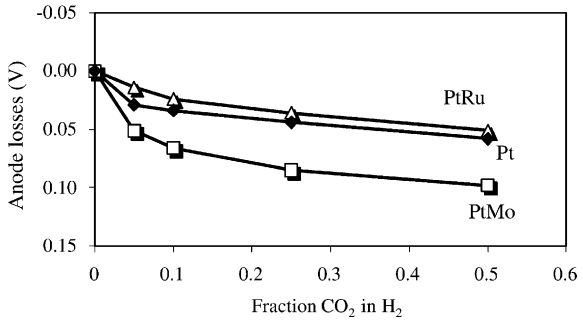

Fig. 7. CO_2 poisoning effect for various anodes using a H_2/CO_2 feed. The figure shows the anode losses at a fixed current density of 350 mA/cm^2 as a function of CO_2 content. Hydrogen stoichiometry 1.5, 80 °C, 1.5 bar gas pressure.

be larger than on Pt. However, it is also quite possible that the rate constant of the RWGS reaction is lower on PtRu. Less interaction with CO may also imply less interaction with CO_2 and intermediates. The final source of increased CO_2 tolerance would be an increased hydrogen dissociation rate. However, Gasteiger et al. [17] found that on Pt and PtRu the electro-oxidation reaction of H_2 was equally fast, and much slower on pure Ru, so it seems this option must be discarded.

PtMo catalysts have a good CO tolerance, which is ascribed to CO electro-oxidation at low (<0.2 V) overpotentials [18]. On the other hand, the CO_2 tolerance is not very good. Ball et al. [11] reported that the CO_2 tolerance decreased in the order PtRu, Pt, PtMo, as corroborated by our results (Fig. 7). Recently, Urian et al. [12] presented more extensive data on CO_2 poisoning of PtRu, Pt, and PtMo catalysts, which showed that at current densities larger than 0.5 A/cm^2 Pt becomes the most CO_2 intolerant species of the three. The structure of the PtMo catalyst surface will depend strongly on the composition as well as the preparation method, which explains differences in CO and CO_2 tolerance observed by different workers. However, in general it is assumed that Mo particles at the surface of both PtMo alloys and bimetallics can easily form (hydro)oxides, which accounts for the easy activation of water, a prerequisite for the electro-oxidation of CO at low overpotential. But the presence of oxidised Mo blocks Pt sites for hydrogen dissociation [18]. Translated to the model presented here this leads to reduced values for the hydrogen dissociation rate k_a, which has a negative effect on the CO_2 tolerance as illustrated by Fig. 4. The observation made by Urian et al. [12] that at high current densities the CO_2 tolerance increases with decreasing Pt:Mo ratio may be related to the oxidation of CO_2 reduction species facilitated by the presence of Mo. The kinetics of CO_2 reduction on supported Pt and PtMo catalysts are at present being studied in our laboratory and will be the subject of a subsequent publication.

In the literature it has been observed that the CO_2 tolerance of anodes also seems to depend on the microstructure. It was concluded that a large fraction of electrochemically inactive particles, i.e. particles not covered by Nafion, increased the CO_2 intolerance [5,19]. An explanation suggested was that electrochemically inactive particles are more active in CO formation as the amount of adsorbed hydrogen would be larger on these particles. This CO would than desorb into the gas phase and poison active particles. In ref. [3] it was shown that electrochemically inactive particles are active catalysts for CO formation from H_2 and CO_2. However, as Fig. 1 shows, at least in the case of a high k_a the values of θ_H and θ_{CO} do not depend much on the current density, i.e. on whether particles are electrochemically active or not. This means that an increased effect of CO formation and desorption into the gas phase from inactive particles is not expected. The analyses presented here rather suggest that the reduced values of the hydrogen dissociation rate k_a, which result for an electrode with an increased fraction of inactive

particles, is the reason for the decrease in CO_2 tolerance. The data presented by Ralph and Hogarth [19] show that the active surface area in various anodes with similar loading can vary by a factor of six, which would correspond to similar variations of k_a. As Fig. 4 shows, a reduction of k_a results in reduced CO_2 tolerance as well as reduced CO formation.

The results have also shown that in true reformate, where CO is present as well as CO_2, that CO_2 will present additional losses, but the losses due to CO and CO_2 are not additive. At high CO content CO_2 reduction cannot take place as there is not sufficient adsorbed hydrogen present on the catalyst.

5. Conclusions

Model calculations have been carried out to study the CO_2 poisoning effect on anode catalyst materials of PEM fuel cells. The main effect of CO_2 poisoning is that due to the RWGS reaction a large part of the catalytic surface area becomes inactive for H_2 dissociation. Subsequent desorption of CO from the catalyst surface, transport down the gas channel, and subsequent re-adsorption of CO plays a minor role. The main reason for this is that a large blockage of the surface area inhibits further formation of CO in the RWGS reaction.

It was found that a high rate constant of the RWGS reaction increases the anode polarisation losses, as does a reduced rate constant of the hydrogen dissociation reaction. The effects are mitigated by a high ratio of the CO desorption and adsorption rate constants, as well as by a high CO electro-oxidation rate constant.

In true reformate where CO is present besides CO_2, CO_2 poisoning will have the largest effect when the CO content is small and at relatively low current density.

Acknowledgements

The author wishes to thank M.P. de Heer for obtaining the data shown in Fig. 7.

References

[1] D.P. Wilkinson, D. Thompsett, in: O. Savadogo, P.R. Roberge (Eds.), New Materials for Fuel Cell and Modern Battery Systems, Proceedings of a Symposium, Ecole Polytechnique, Montreal, PQ, Canada, 1997, p. 266.
[2] T.E. Springer, T. Rockward, T.A. Zawodzinski, S. Gottesfeld, J. Electrochem. Soc. 148 (2001) A11–A23.
[3] M.S. Wilson, C.R. Derouin, J.A. Valerio, S. Gottesfeld, in: Proceedings of the 28th Intersociety Energy Conversion Engineering Conference IECEC, vol. 1, 1993, 1.1203–1.1208.
[4] R.J. Bellows, E.P. Marruchi-Soos, D.T. Buckley, Ind. Eng. Chem. Res. 35 (1996) 1235.
[5] F.A. de Bruijn, D.C. Papageorgopoulos, E.F. Sitters, G.J.M. Janssen, J. Power Sources 110 (2002) 117.
[6] J. Giner, Electrochim. Acta 8 (1963) 857.
[7] D.C. Papageorgopoulos, F.A. de Bruijn, J. Electrochem. Soc. 149 (2002) A140–A145.
[8] M.C. Arévalo, C. Gomis-Bas, F. Hahn, A. Arévalo, A.J. Arvia, Electrochim. Acta 39 (1994) 793.
[9] J. Sobkowski, A. Czerwinski, J. Phys. Chem. 89 (1985) 365.
[10] G.J.M. Janssen, M.P. de Heer, D.C. Papageorgopoulos, in: D. Stolten, B. Emonts, R. Peters (Eds.), Proceedings of the Second European PEFC Forum, Lucerne, Switzerland, 2003, p. 165.
[11] S. Ball, A. Hodgkinson, G. Hoogers, S. Maniguet, D. Thompsett, B. Wong, Electrochem. Solid-State Lett. 5 (2002) A31–A34.
[12] R.C. Urian, A.F. Gulla, S. Mukerjee, J. Electroanal. Chem. 554–555 (2003) 307.
[13] J.J. Baschuk, X. Li, Int. J. Energy Res. 25 (2001) 695.
[14] J. Kim, S.M. Lee, S. Srinivasan, C.E. Chamberlin, J. Electrochem. Soc. 142 (1995) 2670.
[15] B. Hammer, Y. Morikawa, J.K. Nørskov, Phys. Rev. Lett. 76 (1996) 2141.
[16] H. Igarashi, T. Fujino, Y.M. Zhu, H. Uchida, M. Watanabe, Phys. Chem. Chem. Phys. 3 (2001) 306.
[17] H.A. Gasteiger, N.M. Markovic, P.N. Ross, J. Phys. Chem. 99 (1995) 8290.
[18] B.N. Grgur, N.M. Markovic, P.N. Ross Jr., in: S. Gottesfeld, T.F. Fuller, G. Halpert (Eds.), Proton Conducting Membrane Fuel Cells, Second International Symposium, PV 98–27, The Electrochemical Society Proceedings Series, Pennington, NJ, 1999, p. 176.
[19] T.R. Ralph, M.P. Hogarth, Platinum Metal. Rev. 46 (2002) 117.